Nanoscale

Accepted Manuscript

This article can be cited before page numbers have been issued, to do this please use: K. Xi, P. R. Kidambi, R. Chen, G. Chenlong, X. Peng, C. Ducati, S. Hofmann and V. R. Kumar, *Nanoscale*, 2014, DOI: 10.1039/C4NR00326H.

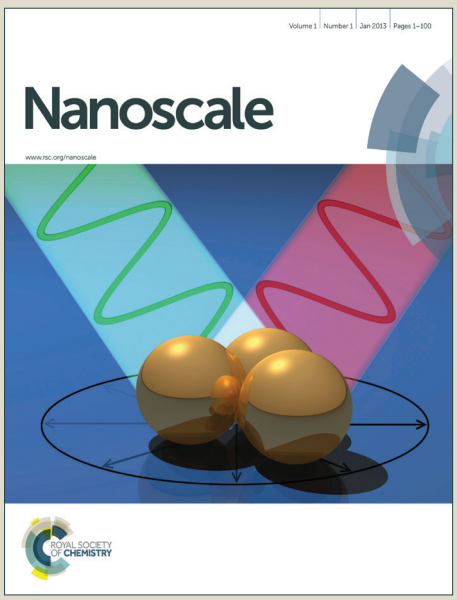

ROYAL SOCIETY OF CHEMISTRY

www.rsc.org/nanoscale

Dynamic Article Links ►
View Article Online
DOI: 10.1039/C4NR00326H

Cite this: DOI: 10.1039/c0xx00000x

www.rsc.org/xxxxxx

ARTICLE TYPE

Binder free three-dimensional sulphur/few-layer graphene foam cathode with enhanced high-rate capability for rechargeable lithium sulphur batteries

Kai Xi,[a‡] Piran R. Kidambi,[b‡] Renjie Chen,[c] Chenlong Gao,[a] Xiaoyu Peng,[a] Caterina Ducati,[a] Stephan Hofmann[b]* and R. Vasant Kumar[a]*

Received (in XXX, XXX) Xth XXXXXXXXX 20XX, Accepted Xth XXXXXXXXX 20XX
DOI: 10.1039/b000000x

A novel ultra-lightweight three-dimensional (3-D) cathode system for lithium sulphur (Li-S) batteries has been synthesised by loading sulphur on to an interconnected 3-D network of few-layered graphene (FLG) via a sulphur solution infiltration method. A free-standing FLG monolithic network foam was formed as a negative of a Ni metallic foam template by CVD followed by etching away of Ni. The FLG foam offers excellent electrical conductivity, an appropriate hierarchical pore structure for containing the electro-active sulphur and facilitates rapid electron/ion transport. This cathode system does not require any additional binding agents, conductive additives or a separate metallic current collector thus decreasing the weight of the cathode by typically ~20-30 wt%. A Li-S battery with the sulphur/FLG foam cathode shows good electrochemical stability and high rate discharge capacity retention for up to 400 discharge/charge cycles at a high current density of 3200 mA g^{-1}. Even after 400 cycles the capacity decay is only ~0.064% per cycle relative to the early (e.g. the 5th cycle) discharge capacity, while yielding an average columbic efficiency of ~96.2%. Our results indicate the potential suitability of graphene foam for efficient, ultra-light and high-performance batteries.

Introduction

There is an increasing demand for lightweight rechargeable batteries to meet the special needs for the next-generation high-performance electronics.[1] Sulphur can react with metallic lithium to form Li_2S with a large negative free energy change, which can be harnessed in a battery with a two-electron reaction with lithium as the anode and sulphur as the cathode. Therefore, a lithium-sulphur (Li-S) battery has a high theoretical specific capacity (1675 mAh g^{-1} of elemental sulphur) and a high nominal energy density (2500 Wh kg^{-1} of cell weight),[2-11] which offers the prospect of a significant energy density improvement compared to the mainstream lithium-ion batteries (150 Wh kg^{-1}).[12-15] Furthermore, elemental sulphur is readily available and poses less risk to the environment than the transition element oxides and phosphates that are currently used in the lithium-ion (Li-ion) batteries.[6, 7] Therefore, sulphur has been considered as a very promising cathode material for the next generation of high energy density rechargeable batteries.

However, the development of Li-S battery technology has been plagued by problems arising from the highly insulating nature of sulphur (5×10^{-30} S cm^{-1} at 25 °C) and the high solubility and diffusivity of lithium polysulphides in the electrolyte.[4, 8, 16, 17] The polysulphides formed as intermediate products from electrochemical reduction of sulphur in the organic electrolyte can diffuse across to cause parasitic reactions resulting in lithium anode corrosion and low columbic efficiency. This redox shuttle mechanism[16, 18, 19] is mainly responsible for the commonly observed poor cycle life of Li-S batteries. To address these issues, several scientific and technological innovations have been proposed which include forming a protective film on the lithium anode,[20] optimizing the electrolyte,[21, 22] and fabricating composite electrodes of sulphur/polymer[23-26], sulphur/metal organic framework (MOF)[8, 27] and sulphur/carbon[8, 16, 28-36].

Recently, graphene powder, a material with a high conductivity and large theoretical surface-area, has been employed in combination with sulphur to form a cathode for a Li-S battery.[32, 35-42] Graphene oxide has also been used to confine the diffusion of polysulfides, to overcome the poor cycle performance of the sulphur based cathode but its conductivity is much lower than graphene.[32, 34, 42] However, most of the reported cathodes formulated using graphene powder and sulphur as starting materials have required the use of polymeric binders and carbon black additives to ensure mechanical stability and electrical connectivity of the composite. Hence, the overall energy density of resulting electrodes is reduced by the increased weight of the cathode due to carbon black additives[32, 34, 37-39, 42] (typically ~10-20 wt%) and binders[32, 34, 37-42] (typically ~10 wt%). Further, these composites contain many interfaces and grain boundaries resulting in several irregularly connected carbon

View Article Online
DOI: 10.1039/C4NR00326H

networks. These interfaces act as scattering centres for electron transport leading to increased internal resistances of the cathode of a Li-S battery. Therefore, binder and carbon additive – free cathode can offer flexibility in developing new porous cathode designs. In recent times, binder-free graphene/sulfur composite materials have been reported as a cathode in Li-S battery system, which demonstrate a great potential of using graphene to load sulphur as a novel cathode structure. [36, 43]

In this work, we report on the design of an ultra-light Li-S battery cathode based on loading sulphur onto a free-standing porous and interconnected 3-D network of FLG foam via a sulphur solution infiltration method. The FLG foam is synthesised by chemical vapour deposition (CVD) from a catalyst metal template, which is scalable and emerging as one of the most promising routes to high quality graphene production.[44-46] The excellent electrical conductivity and 3-D interconnected structure of the FLG foam facilitates rapid electron and ion transport. Departing from the normal practice in conventional Li-S batteries, we have been able to eliminate additional components such as metal current collectors, conducting additives such as C-black and binders such as polytetrafluoroethene (PTFE) from the cathode system. The sulphur/FLG foam 3-D network structure shows excellent high-rate cycle stability and high columbic efficiency over 400 cycles when used as a cathode in a Li-S battery.

Experimental

Preparation and characterization

A few-layered graphene (FLG) foam was synthesised by CVD via a sacrificial Ni foam template (Alantum Europe GmbH, pore size ~450 µm, area density 420 gm^{-2} and thickness 1.6 mm) from CH_4 and H_2 at atmospheric pressure in a hot walled tube furnace at a 1000°C. [44-47] After the CVD growth process, the FLG covered Ni scaffold was trimmed along the edges to create access for the etchant and the scaffold was subsequently etched using 0.5 M $FeCl_3$ solution to obtain free-standing FLG foam. This was followed by repeated washing in deionised (DI) water and a final etch in 10% HCl to remove trace Fe contamination. The FLG foam was then washed again in DI water and subsequently rinsed in iso-propanol (IPA) and left to dry in ambient air.

Elemental sulphur powder (99.98%, Aldrich) and the FLG foam were dried in vacuum at 80 °C before use. Then, 0.1 g sulphur was dissolved in 30 mL toluene (Sigma-Aldrich, 99.8%, anhydrous). The sulphur/FLG foam cathodes were prepared by infiltrating the sulphur solution into the FLG foam by drop casting. More specifically sulphur solution was dropped onto the FLG foam and then allowed to dry for a few minutes. The sulphur content in sulphur/FLG foam composites was calculated by the mass change in the FLG foam before and after sulphur infiltration. The process of drop coating was repeated until the amount of sulphur required was added to the graphene structure. The loading density of sulfur was approximately 2.0 mg/cm^2. The amount of sulphur introduced could be controlled by varying either the concentration of sulphur in the toluene solution and/or by repeating the drop casting process.

X-ray diffraction patterns were collected using a Bruker D8-advance powder X-ray diffractometer with a Cu K-α source operated at a power of 1600 W (40 mA, 40 kV). Scanning electron microscopy (SEM) and energy dispersive X-ray spectroscopy (EDX) were performed in a Philips XL 30 SEM and/or a JEOL 5800 LV SEM. Raman spectra were measured using a Renishaw In-Via spectrometer with a 532 nm wavelength laser. 4 probe devices were fabricated using silver paste to contact wires to the FLG foam and measured using a Keithley source measurement unit. Transmission electron microscope (TEM, FEI Tecnai F20-G2 FEGTEM) was performed by preparing a dilute ethanol suspension of the as-prepared FLG foam via ultrasonic dispersion and drop casting it on a copper grid covered with a carbon film. The surface area of the FLG foam was estimated using the Brunauer–Emmett–Teller (BET) equation for the relative pressure range (P/P_o) of 0.002 to 0.3. The saturation pressure, P_o, corresponds to approx. 103.4 kPa. Non-local density functional theory (NLDFT) calculation was used to generate the pore size distribution data, based on the carbon slit pores geometry assumption.

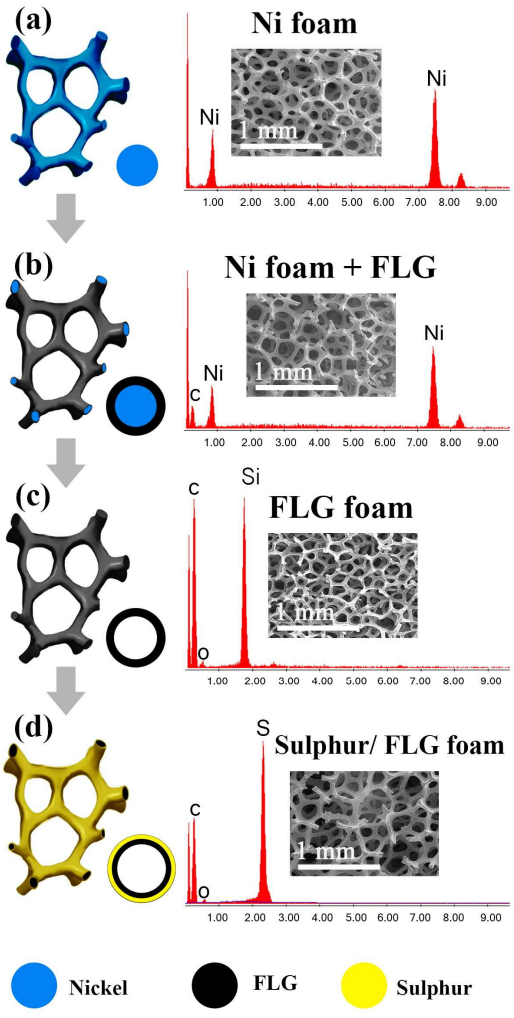

Figure 1. Schematic representation of the different steps in the synthesis of the sulphur/FLG foam composite along with SEM images and EDX spectra of the (a) Ni foam, (b) post FLG CVD on the Ni foam, (c) free standing FLG foam after Ni scaffold etching and (d) sulphur/FLG foam. The Si and O peaks in the EDX come from the Si/SiO_2 (300 nm) wafer used to support the sample in the SEM.

View Article Online
DOI: 10.1039/C4NR00326H

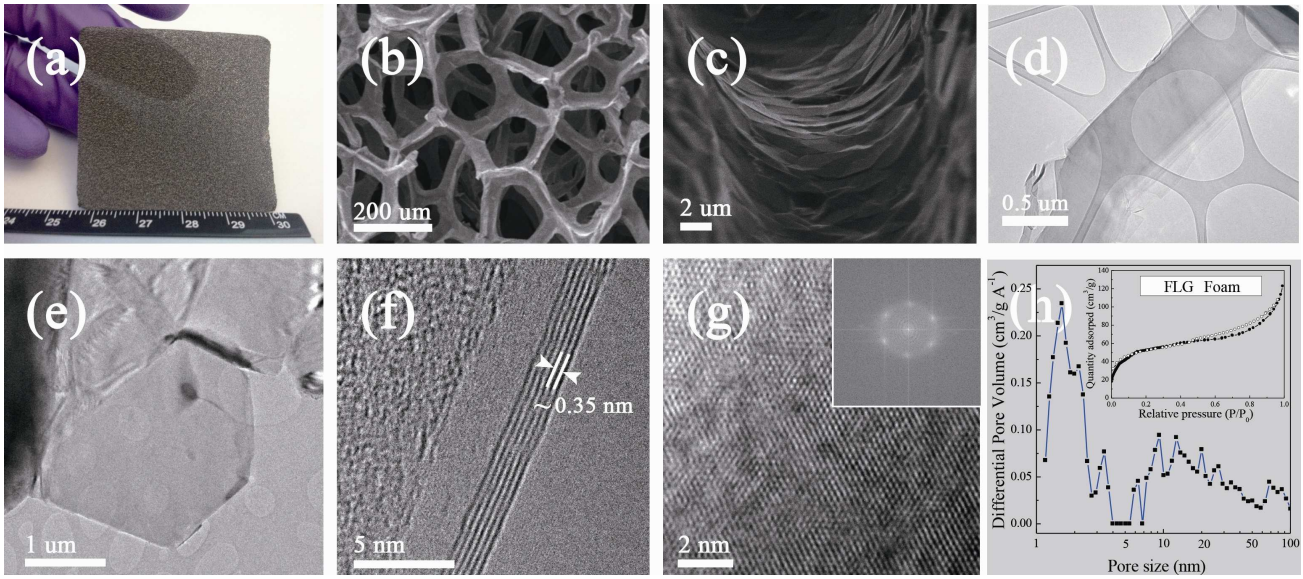

Figure 2. (a) A photograph of a 45x45 mm^2 free-standing FLG foam. (b), (c) SEM images of the FLG foam at low and higher magnification. (d), (e) Low-magnification TEM images of the FLG foam. High-resolution TEM images of the FLG foam (f) cross section and (g) lattice fringes with FFT in the inset. h) N_2 adsorption/desorption isotherms of the sample (adsorption: ●; desorption: ○), and their corresponding pore size distribution.

Electrochemical measurements

Lithium batteries were assembled in a glove box under argon atmosphere. Lithium metal (99.99%, Sigma-Aldrich) was used as the anode and the reference electrode. The separator was a commercial micro-porous polypropylene product (Celgard 2400). Copper foil was used as the anode current collector while no cathode current collector was required as the monolithic graphene network was able to provide this function. 1.0 M $LiN(CF_3SO_2)_2$ (1 M) (99.95%, trace metals basis, Sigma-Aldrich) salt dissolved in a mixture of dioxolane (DOL) (99.8%, Sigma-Aldrich) and 1,2-dimethoxyethane (DME) (99.5, Sigma-Aldrich) in a volume ratio of 1:1 containing $LiNO_3$ (1 wt%) was used as the electrolyte. Galvanostatic charge/discharge tests were performed to evaluate the electrochemical capacity and cycle life of the electrodes at room temperature using a LAND-CT2001A instrument (Wuhan, China).

Results and discussion

Figure 1 shows a schematic overview of the different stages involved in the synthesis of the sulphur/FLG foam along with EDX spectra and SEM images of each stage. A Ni foam scaffold was used as a catalyst template for graphene CVD. The initial Ni foam shows only Ni (EDX peaks at ~ 0.8, 7.5 and 8.2 kV, Fig. 1a). After the CVD process, a carbon peak (~0.2 kV) along with the Ni peaks is observed in the EDX spectra while the 3-D foam structure is preserved (Fig. 1b). The subsequent removal of the Ni scaffold gives rise to a free standing hollow interconnected 3-D FLG foam and EDX spectra show only peaks corresponding to carbon and no peaks for Ni, indicating that the etching was complete and effective (Fig. 1c). We note that additional peaks for Si (1.7 kV) and O (0.5 kV) are attributed to the Si/SiO_2 wafer on which this particular sample was mounted to obtain SEM images. Upon sulphur infiltration, the EDX spectra of sulphur/FLG foam confirm the presence of sulphur (~2.2 kV) and carbon and the SEM images show that the resulting sulphur/FLG foam retains the interconnected 3-D composite network (Fig. 1d).

We further characterized the FLG structures using optical microscopy, SEM, TEM and N_2 adsorption/desorption isotherms. Fig. 2a and 2b show that the FLG foam has an integrated 3-D macro-porous structure with pore diameter of ~50–200 μm providing a stable reservoir for electrolyte. However, the higher magnification SEM image (Fig. 2c) shows large surface ripples and wrinkles in the FLG. Such morphology can favour uniform sulphur loading on to the FLG foam by our facile solution infiltration method (see Fig 3a-c below). Low-magnification TEM images (Fig. 2d and 2e) show a continuous sheet/film like morphology, which could be due to the dispersion of the FLG foam in ethanol for drop casting on the TEM grid. The high-resolution cross-sectional TEM image (Fig. 2f) shows ~5 graphene layers stacked on top of each other with a spacing of ~0.34 - 0.35 nm. Top view TEM imaging (Fig. 2g) clearly shows a graphitic hexagonal honeycomb lattice and a fast Fourier transform shows diffraction spots consistent with FLG (see inset). This is further corroborated by Raman spectroscopy (Figure 4e) which shows distinct 2D (~2700 cm^{-1}) and G (1600 cm^{-1}) peaks with a I_G/I_{2D} ratio >1 and a 2D peak that cannot be fitted with a single Lorentzian peak, as expected for FLG.[48] There is no observable D (~1350 cm^{-1}) peak, indicative of the high crystalline quality.[48] N_2 physisorption measurements give sorption isotherms (Fig. 2h inset) at 77 K which is a combination of Type I, characteristic of microporous materials, and Type IV, characteristic of mesoporous materials. Besides, type H3 adsorption hysteresis loops, without any limiting adsorption at high p/p^o, are observed with aggregates of plate-like particles rise to slit-shape pores.[49] It further demonstrates the layered structure of FLG. Additionally, the FLG foam shows a hierarchically porous structure (Fig.2 h) with a surface area of 160 m^2 g^{-1}. It exhibits micro- (< 2 nm), meso- (2–50 nm), and macropores (>50 nm) structure with a rather high proportion of micropores which is known to help improve cycle-life by retaining polysulphides in such pores.[8, 31, 50, 51] As deduced from transmission electron microscope image analysis, the formation of the nanoporous structure could arise from two potential schemes (Fig. 3). The staggered stacking like morphology of the FLG multi-layer sheets can be clearly observed in the TEM images (Fig.3a inset and Fig

View Article Online
DOI: 10.1039/C4NR00326H

S1). As shown, FLGs are stacked with either staggered orientations which is similar to stacked envelopes (Fig. S1a) or as wrinkled plates with undulating surface of FLG (Fig. 3b inset). Both Fig. 3a and 3b provide explanations for the formation of stable hierarchical porous structures. These variations in textural characteristics were further studied to reveal the underlying relationship between the FLG textures and the Li–S battery capacities/cycle stabilities.

SEM images in Fig. 4a and 4d show the change in surface morphology upon infiltration with 52 wt% sulphur. The wrinkles and ripples observed earlier on the FLG (Fig. 2c) are no longer seen. An EDX elemental map for carbon (Fig. 4b) and sulphur (Fig. 4c) corresponding to the SEM image in Figure 4a indicate a uniform distribution of sulphur across the surface of the FLG foam. This is further confirmed by Raman spectroscopy (Fig. 4e) where the 52 wt% sulphur/FLG foams clearly showed distinct peaks at ~153, ~218 and ~473 cm^{-1} corresponding to elemental sulphur.[52]

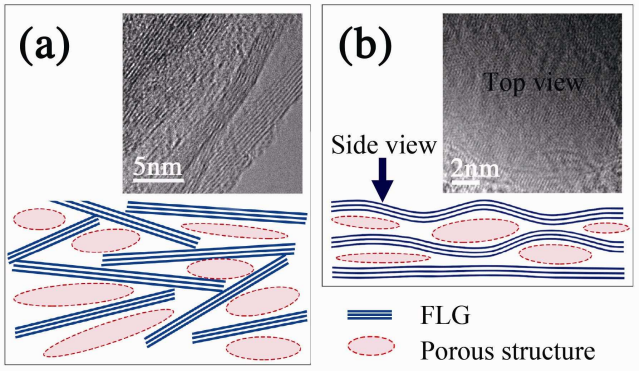

Figure 3. TEM images of FLG foam with pictorial mechanism schemes for forming hiearchical porous structure.

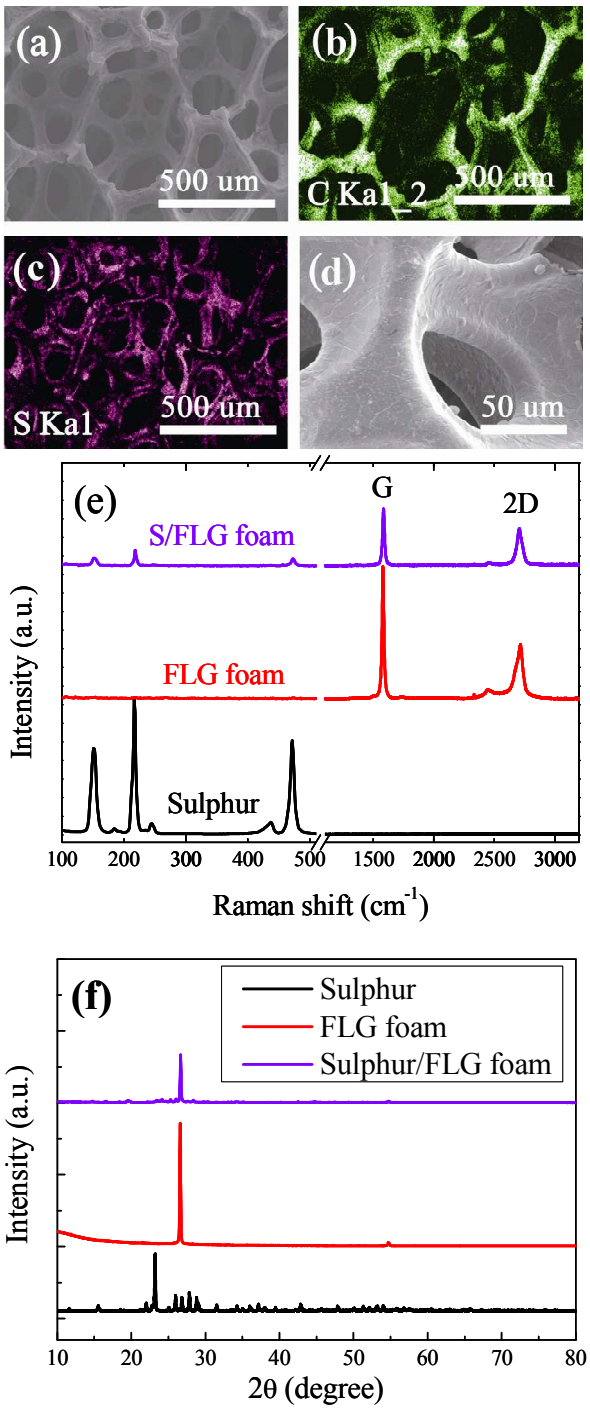

Figure 4. SEM images of sulphur/FLG foam with 52 wt% sulphur at (a) low and (d) high magnification shows the change in surface morphology upon sulphur infiltration. EDX elemental maps of (b) carbon and (c) sulphur corresponding SEM image in Fig. 4 (a) showing the uniform distribution of sulphur across the surface of the FLG foam. (e) Raman spectra and (f) XRD pattern for sulphur, the FLG foam and the sulphur/FLG composite.

View Article Online
DOI: 10.1039/C4NR00326H

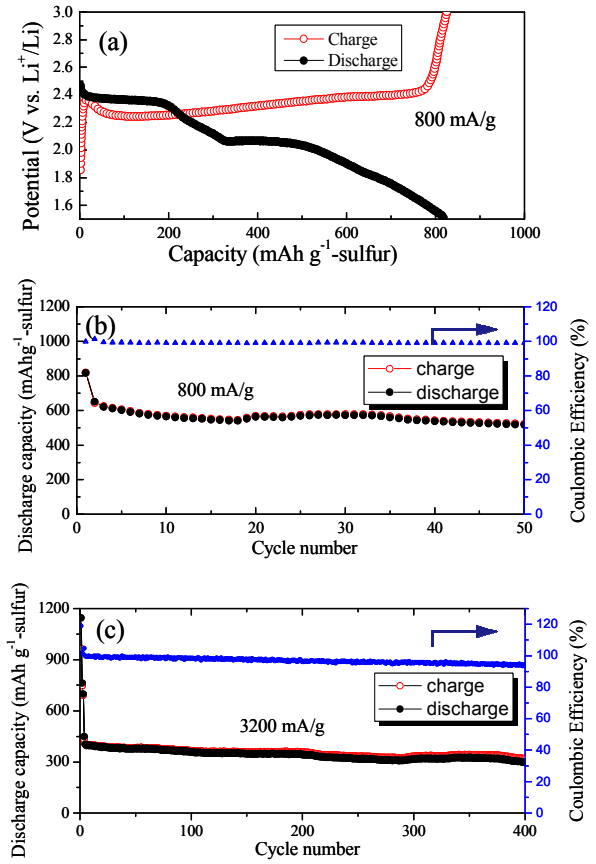

Figure 5. Rate and cyclic performance of the sulphur/FLG foam composites with 52 wt% sulphur. (a) Initial discharge/charge curves and (b) cycle performance of samples at a specific current of 800 mA g^{-1}. (c) Capacity of the battery charged/discharged at a constant specific current of 3200 mA g^{-1} for 400 cycles after activation at 400 mA g^{-1} during the 4 initial cycles. The electrochemistry test is between 1.5 and 3.0 V (vs Li^+/Li) in the electrolyte ($LiN(CF_3SO_2)_2$/ DOL:DME=1:1(v/v)) containing $LiNO_3$ (1 wt%).

To investigate the process of infiltration of sulphur, X-ray diffraction (XRD) patterns of the elemental sulphur, FLG, sulphur/FLG composites infiltrated with 52 wt% sulphur were performed (Fig. 4f). While sharp diffraction peaks are seen for pure sulphur powder (indicating the presence of elemental sulphur in a crystalline state with an orthorhombic structure) and the FLG foam (peaks ~26° and ~55° corresponding to graphite reflections), no sulphur related reflections are seen for the sulphur/FLG composite. During the drop casting based infiltration of sulphur on FLG, elemental sulphur is expected to diffuse into the pores and coat the graphene surface. The combination of XRD patterns with the SEM image (Fig. 4d), Raman and the EDX maps (Figs. 4a, b and c) indicate that the sulphur might be a in highly dispersed amorphous state[31] not detectable by XRD but clearly seen in the EDX and Raman spectra.

The composite was incorporated as a cathode in a Li-S battery and Fig. 5a shows initial discharge/charge curves for cells at a specific current of 800 mA g^{-1} with the sulphur/FLG foam composite as a working electrode containing 52 wt% sulphur in an electrolyte made of 1.0 M $LiN(CF_3SO_2)_2$ salt dissolved in a mixture of dioxolane (DOL) and 1,2-dimethoxyethane (DME) at a volume ratio of 1:1 containing $LiNO_3$ (1 wt%). An initial discharge capacity of 820 mAh g^{-1} was observed. The discharge curve demonstrates three main potential regions. The first region is nearly a plateau at 2.4 V, a second region sloping down from 2.4–2.1 V and a third region as a plateau at 2.1 V (vs. Li/Li^+). These signatures correspond to the formation of long-chain soluble lithium polysulfides (Li_2S_n; where n is typically 4–8) in the first 2-regions and short-chain solid sulphides (Li_2S_2 and Li_2S) in the final plateau.[16, 19, 53]

It should be noted that the first main plateau is observed clearly, indicating that sulphur containing compounds is entrenched in the various hierarchical nano-pores of the FLG foam, such that a two-phase region exists in the early part of the discharge cycle. The ability to sequester higher-order polysulfides within the cathode is considered critical for improving cycle life. The potential hysteresis phenomenon is observed in the low potential plateau, which is typically presented in micro-pore rich cathodes.[8, 31, 50, 54] The low potential reduction could be due to the extra electrode polarization required to overcome the nanoconfinement barrier of strong adsorption energy.[8, 31, 50, 54] Sulphur embedded in the narrow pores of FLG undergoing electrochemical reaction during the discharge process needs to overcome the absorbing energy, leading to the observed discharge potential hysteresis. On the other hand, it is also noted that the low-molecular (S_{2-4}) forms of elemental sulphur in a high dispersion state and a short chain configuration inside the narrow micropores are unstable due to their high energy state (low potential difference versus metallic lithium) as compared to large molecules of elemental sulfur with crown rings, which leads to the electrochemical reduction process starting from S_{2-4} to S^{2-}.[31, 50] Such behaviour will also result in the observed discharge potential hysteresis.

Fig. 5b shows the cycling behaviour of the sample at 800 mA g^{-1}. After an initial capacity loss during the settling of the battery, the sulphur/FLG composites exhibited good capacity retention upon cycling. The capacity was found to stabilize at 518 mAh g^{-1} at the current density of 800 mA g^{-1} after 50 full cycles. This can translate to 1.04 mAh/cm^2 of area capacity, which is comparable with previous reports (Fig. S2).[55] An average coulombic efficiency, calculated as the ratio of discharging and charging capacity, of 99.2 % is achieved indicating reversibility of the electrochemical reactions and excellent capacity retention.

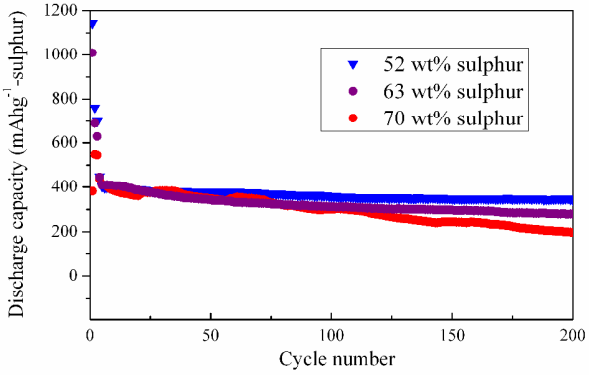

Figure 6. Cycle performances of the sulphur/FLG foam with 52 wt % S , 63 wt % S and 70 wt % S in the electrolyte ($LiN(CF_3SO_2)_2$/ DOL:DME=1:1(v/v)) containing $LiNO_3$ (1 wt%) at the current density of 3200 mA g^{-1}

View Article Online
DOI: 10.1039/C4NR00326H

Fig. S3 shows galvanostatic measurements of the high-rate capacity of the samples at room temperature with increasing values of charge/discharge current densities of 400, 800, 1600 and 3200 mA g^{-1} applied successively. The cell was discharged and charged over cycles at different current densities, followed by recording the discharge/charge curves. The same pattern of discharge and charge voltage plateaus even at very high current densities is observed, providing evidence for identical electrochemical processes at all current densities. The cycle performance of the cells at a high current density is illustrated in Fig. 5c. These results indicate the abuse tolerance of the battery when subject to high current drain or power usage. The superior high-rate discharge capability of the cathode is ascribed to fast charge-transfer kinetics arising from the high electrical (electronic and ionic) conductivity of the 3-D FLG foam network. After conditioning the cell at 400 mA g^{-1} for 4 cycles, the electrode was discharged and charged at 3200 mA g^{-1}. An initial discharge capacity of 1143 mAh g^{-1}, which is ~68% of the theoretical capacity, is observed. At the current density of 3200 mA g^{-1}, the measured discharge capacity is 402.8 mAh g^{-1} in the 5th cycle. Furthermore, after the 400th cycle using a high current density of 3200 mA g^{-1}, the present working electrode still retained a discharge capacity of ~300 mAh g^{-1}, which corresponds to a decay of only 0.064% per cycle when compared with discharge capacity at the 5th cycle. This represents good electrochemical stability and high rate discharge capacity retention (i.e. up to 400 discharge/charge cycles) of the Li-S batteries. The composite also shows a coulombic efficiency as high as 94.6% after 400 cycles at high current. The average coulombic efficiency is calculated to be 96.2%, indicating reliable stability.

To further understand the sulfur loading ability of FLG foam, the composites with 63 and 70 wt % at the current density of 3200 mA g^{-1} after conditioning for 4 cycles are presented in Fig. 6. The composite with 63 wt% sulphur still presented good initial discharge capacity of 1008 mAh g^{-1} with good cycle stability after 200 cycles. When the sulphur content was increased to 70 wt%, both initial discharge capacity and the cycle stability deteriorated due to the pore- narrowing and full saturation of the micropores, which prevent passage of solvated electrolyte molecules. Therefore, the sulphur/FLG composite with appropriate sulphur content, normalized with respect to the total cathode weight can endure high current densities and yet retain good stability upon cycling. This is advantageous for abuse tolerance of lithium batteries with high power and long cycle life. The improved high-rate capability of our samples is attributed to the fast charge-transfer kinetics arising from the interconnected structure of the FLG foam.

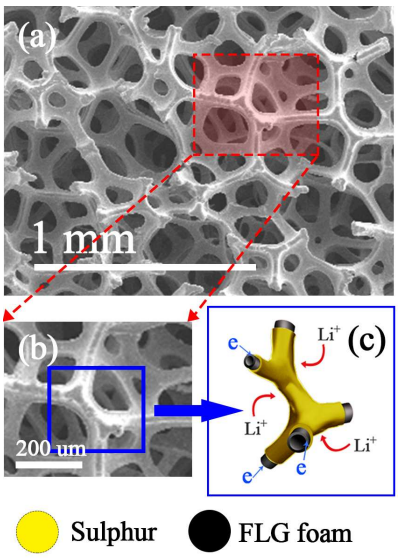

Figure 7. SEM images (a, b) and a scheme of the fast charge-transfer kinetics (c) inside the sulphur/FLG foam cathode.

The 3-D sulphur/FLG composite provides not only high rate cycle stability for the Li-S battery, but also good columbic efficiencies, due to the structural features of the FLG foam. Figure 7 outlines a proposed electron transfer model to rationalise the experimental observations above. The FLG foam in principle works as a current collector which when loaded with sulphur can be used as a cathode for Li-S batteries. The excellent electrical conductivity and interconnected 3-D network of the electrode enable rapid electron and ion transport at the FLG/electrolyte interfaces. The conductivity of the FLG foam at ~2.25 S cm^{-1} (measured using a 4 point probe method and using the thickness of the foam i.e. 1.6 mm) further supports this hypothesis. We note that this value of conductivity is consistent with other reports in literature[44, 56] and is much higher than for reduced graphene oxide, carbon nanofibers and other carbon materials used for Li-S batteries reported earlier.[35, 36] Furthermore, micropores (< 2 nm) help improve cycle life by effectively confining polysulfide anion diffusion in the organic electrolyte.[8, 31, 50] Since the proportion of micropore is quite large in the FLG foam, stability in cycle life is also observed. We emphasise that electrochemical performance achieved in the sulphur/FLG composite is without metal current collectors, conducting additives, and binders. Beside, the capacity is comparable with the reports in literatures and the long cycle rate performance even better.[32, 34-38]

We propose the initial irreversible reaction probably occurs at the sulphur-FLG interface due to the favourable electron transport from conductive FLG to sulphur. The capacity loss in the following cycles is due to the solution and diffusion of some of the polysulphides (in the 2nd voltage region) and thus the polysulphides cannot be completely converted into elemental sulphur in the oxidation process during charging.[3, 9-11, 53] While the FLG foam only has a relatively low surface area of ~160 m^2/g, thus resulting in relatively lower discharge capacity, especially in the lower potential plateau.[16, 57] But the composite network presents excellent electrochemical stability and high rate discharge capacity retention, from the 3-D foam micro-porous structure. The network provides a direct conductive pathway for the rapid ion-electron exchange and external electron transport.

View Article Online
DOI: 10.1039/C4NR00326H

Further exploration and improvement of sulphur cathode composites would be an important step towards the development of future high energy rechargeable battery system. A significant weight reduction from removal of additional metal current collectors, conducting additives or binders can be achieved. The excellent electrical conductivity and pore structure of the FLG network can be used in many other hybrid electrode applications. To cope with the lower capacity issues, hybrid structures combining both FLG foam and other high surface area conductive materials are currently being investigated.

Conclusions

In summary, we have developed an ultra-lightweight 3-D sulphur/FLG foam lithium-sulphur battery cathode, which does not requires any metal current collectors, or conducting additives, and binders, thus offering comparable or better sulphur loading with respect to total cathode weight. The as-prepared electrode composite demonstrated excellent high-rate discharge stability as cathode in a Li-S cell. The improved high-rate capability is attributed to fast charge-transfer kinetics enabled by the conductive interconnected FLG foam network with high electrical conductivity. Compared with the 5th cycle discharge capacity, the capacity decay is as small as 0.064% per cycle at a high current density of 3200 mA g^{-1} and an average coulombic efficiency of 96.2 % over 400 cycles. The results show that loading electrode materials on a free-standing interconnected FLG foam network can be a promising design for rechargeable batteries with high rate performance. We plan further studies of other form factors and loadings to increase the overall capacity of such batteries.

Acknowledgements

Kai Xi thanks the Cambridge Overseas Trust. P.R.K. acknowledges funding from the Cambridge Commonwealth Trust. S.H. acknowledges funding from ERC grant InsituNANO (no. 279342), EPSRC under grant GRAPHTED (project reference EP/K016636/1) and Grant EP/H047565/1. This research was partially supported by the EU FP7 Work Programme under grant GRAFOL (project reference 285275). XP and CD acknowledge funding from the ERC under grant number 259619 PHOTO EM.

Notes and references

[a] *Department of Materials Science and Metallurgy, University of Cambridge, Cambridge, CB2 3QZ, UK. Fax: +44 (0)1223 334567; Tel: +44 (0)1223 334327; E-mail: rvk10@cam.ac.uk*
[b] *Department of Engineering, University of Cambridge, Cambridge, CB3 0FA, UK. Fax: +44 (0)1223 748348; Tel: +44 (0)1223 748346; E-mail: sh315@cam.ac.uk*
[c] *School of Chemical Engineering and Environment, Beijing Institute of Technology, Beijing, 100081, China*
‡***both authors contributed equally to this work***

1. N. Li, Z. Chen, W. Ren, F. Li and H.-M. Cheng, *Proceedings of the National Academy of Sciences*, 2012, **109**, 17360-17365.
2. X. Ji and L. F. Nazar, *Journal of Materials Chemistry*, 2010, **20**, 9821-9826.
3. P. G. Bruce, S. A. Freunberger, L. J. Hardwick and J.-M. Tarascon, *Nat Mater*, 2012, **11**, 19-29.
4. R. D. Rauh, K. M. Abraham, G. F. Pearson, J. K. Surprenant and S. B. Brummer, *J. Electrochem. Soc.*, 1979, **126**, 523-527.
5. H. Yamin and E. Peled, *Journal of Power Sources*, 1983, **9**, 281-287.
6. P. Novák, K. Müller, K. S. V. Santhanam and O. Haas, *Chemical Reviews*, 1997, **97**, 207-282.
7. D. Marmorstein, T. H. Yu, K. A. Striebel, F. R. McLarnon, J. Hou and E. J. Cairns, *Journal of Power Sources*, 2000, **89**, 219-226.
8. K. Xi, S. Cao, X. Peng, C. Ducati, R. Vasant Kumar and A. K. Cheetham, *Chemical Communications*, 2013, **49**, 2192-2194.
9. M.-K. Song, E. J. Cairns and Y. Zhang, *Nanoscale*, 2013, **5**, 2186-2204.
10. Y. Yang, G. Y. Zheng and Y. Cui, *Chem. Soc. Rev.*, 2013, **42**, 3018-3032.
11. A. Manthiram, Y. Fu and Y.-S. Su, *Accounts of Chemical Research*, 2012, **46**, 1125-1134.
12. J. Hassoun and B. Scrosati, *Angewandte Chemie International Edition*, 2010, **49**, 2371-2374.
13. B. Scrosati, J. Hassoun and Y.-K. Sun, *Energy & Environmental Science*, 2011, **4**, 3287-3295.
14. K. E. Aifantis, S. A. Hackney and R. V. Kumar, *High Energy Density Lithium Batteries: Materials, Engineering, Applications*, John Wiley & Sons, 2010.
15. X. P. Gao and H. X. Yang, *Energy & Environmental Science*, 2010, **3**, 174-189.
16. J. Shim, K. A. Striebel and E. J. Cairns, *J. Electrochem. Soc.*, 2002, **149**, A1321-A1325.
17. C. Barchasz, J.-C. Leprêtre, F. Alloin and S. Patoux, *Journal of Power Sources*, 2012, **199**, 322-330.
18. J. R. Akridge, Y. V. Mikhaylik and N. White, *Solid State Ionics*, 2004, **175**, 243-245.
19. Y. V. Mikhaylik and J. R. Akridge, *J. Electrochem. Soc.*, 2004, **151**, A1969-A1976.
20. L. Yong Min, C. Nam-Soon, P. Jung Hwa and P. Jung-Ki, *Journal of Power Sources*, 2003, **119-121**, 964-972.
21. D. Aurbach, E. Pollak, R. Elazari, G. Salitra, C. S. Kelley and J. Affinito, *J. Electrochem. Soc.*, 2009, **156**, A694-A702.
22. X. Liang, Z. Wen, Y. Liu, M. Wu, J. Jin, H. Zhang and X. Wu, *Journal of Power Sources*, 2011, **196**, 9839-9843.
23. J. L. Wang, J. Yang, J. Y. Xie and N. X. Xu, *Advanced Materials*, 2002, **14**, 963-965.
24. M. Sun, S. Zhang, T. Jiang, L. Zhang and J. Yu, *Electrochemistry Communications*, 2008, **10**, 1819-1822.
25. X. Liang, Y. Liu, Z. Wen, L. Huang, X. Wang and H. Zhang, *Journal of Power Sources*, 2011, **196**, 6951-6955.
26. F. Wu, J. Chen, R. Chen, S. Wu, L. Li, S. Chen and T. Zhao, *The Journal of Physical Chemistry C*, 2011, **115**, 6057-6063.
27. R. Demir-Cakan, M. Morcrette, F. Nouar, C. Davoisne, T. Devic, D. Gonbeau, R. Dominko, C. Serre, G. Ferey and J. M. Tarascon, *J. Am. Chem. Soc.*, 2011, **133**, 16154-16160.
28. J. Wang, S. Y. Chew, Z. W. Zhao, S. Ashraf, D. Wexler, J. Chen, S. H. Ng, S. L. Chou and H. K. Liu, *Carbon*, 2008, **46**, 229-235.
29. N. Jayaprakash, J. Shen, S. S. Moganty, A. Corona and L. A. Archer, *Angewandte Chemie International Edition*, 2011, **50**, 5904-5908.
30. X. Ji, K. T. Lee and L. F. Nazar, *Nat Mater*, 2009, **8**, 500-506.

View Article Online
DOI: 10.1039/C4NR00326H

31. B. Zhang, X. Qin, G. R. Li and X. P. Gao, *Energy & Environmental Science*, 2010, **3**, 1531-1537.
32. H. L. Wang, Y. Yang, Y. Y. Liang, J. T. Robinson, Y. G. Li, A. Jackson, Y. Cui and H. J. Dai, *Nano Letters*, 2011, **11**, 2644-2647.
33. S. Doerfler, M. Hagen, H. Althues, J. Tuebke, S. Kaskel and M. J. Hoffmann, *Chemical Communications*, 2012, **48**, 4097-4099.
34. N. Li, M. Zheng, H. Lu, Z. Hu, C. Shen, X. Chang, G. Ji, J. Cao and Y. Shi, *Chemical Communications*, 2012, **48**, 4106-4108.
35. S. Lu, Y. Cheng, X. Wu and J. Liu, *Nano Letters*, 2013, **13**, 2485-2489.
36. G. Zhou, L.-C. Yin, D.-W. Wang, L. Li, S. Pei, I. R. Gentle, F. Li and H.-M. Cheng, *ACS Nano*, 2013, **7**, 5367-5375.
37. J. Z. Wang, L. Lu, M. Choucair, J. A. Stride, X. Xu and H. K. Liu, *Journal of Power Sources*, 2011, **196**, 7030-7034.
38. Y. L. Cao, X. L. Li, I. A. Aksay, J. Lemmon, Z. M. Nie, Z. G. Yang and J. Liu, *Phys. Chem. Chem. Phys.*, 2011, **13**, 7660-7665.
39. B. Wang, K. F. Li, D. W. Su, H. J. Ahn and G. X. Wang, *Chem.-Asian J.*, 2012, **7**, 1637-1643.
40. T. Lin, Y. Tang, Y. Wang, H. Bi, Z. Liu, F. Huang, X. Xie and M. Jiang, *Energy & Environmental Science*, 2013, **6**, 1283-1290.
41. S. Evers and L. F. Nazar, *Chemical Communications*, 2012, **48**, 1233-1235.
42. L. W. Ji, M. M. Rao, H. M. Zheng, L. Zhang, Y. C. Li, W. H. Duan, J. H. Guo, E. J. Cairns and Y. G. Zhang, *J. Am. Chem. Soc.*, 2011, **133**, 18522-18525.
43. J. Jin, Z. Wen, G. Ma, Y. Lu, Y. Cui, M. Wu, X. Liang and X. Wu, *RSC Advances*, 2013, **3**, 2558-2560.
44. Z. Chen, W. Ren, L. Gao, B. Liu, S. Pei and H.-M. Cheng, *Nat Mater*, 2011, **10**, 424-428.
45. P. R. Kidambi, B. C. Bayer, R. S. Weatherup, R. Ochs, C. Ducati, D. V. Szabó and S. Hofmann, *physica status solidi (RRL) – Rapid Research Letters*, 2011, **5**, 341-343.
46. P. R. Kidambi, C. Ducati, B. Dlubak, D. Gardiner, R. S. Weatherup, M.-B. Martin, P. Seneor, H. Coles and S. Hofmann, *The Journal of Physical Chemistry C*, 2012, **116**, 22492-22501.
47. R. S. Weatherup, B. C. Bayer, R. Blume, C. Baehtz, P. R. Kidambi, M. Fouquet, C. T. Wirth, R. Schlögl and S. Hofmann, *ChemPhysChem*, 2012, **13**, 2544-2549.
48. A. C. Ferrari, *Solid State Communications*, 2007, **143**, 47-57.
49. K. S. W. Sing, D. H. Everett, R. A. W. Haul, L. Moscou, R. A. Pierotti, J. Rouquerol and T. Siemieniewska, *Pure and Applied Chemistry*, 1985, **57**, 603-619.
50. S. Xin, L. Gu, N.-H. Zhao, Y.-X. Yin, L.-J. Zhou, Y.-G. Guo and L.-J. Wan, *J. Am. Chem. Soc.*, 2012, **134**, 18510-18513.
51. G. Liu, Z. Su, S. Sarfraz, K. Xi and C. Lai, *Materials Letters*, 2012, **84**, 143-146.
52. A. T. Ward, *The Journal of Physical Chemistry*, 1968, **72**, 4133-4139.
53. S. S. Zhang, *Journal of Power Sources*, 2013, **231**, 153-162.
54. D.-W. Wang, G. Zhou, F. Li, K.-H. Wu, G. Q. Lu, H.-M. Cheng and I. R. Gentle, *Phys. Chem. Chem. Phys.*, 2012, **14**, 8703-8710.
55. T. Xu, J. Song, M. L. Gordin, H. Sohn, Z. Yu, S. Chen and D. Wang, *ACS Applied Materials & Interfaces*, 2013, **5**, 11355-11362.
56. F. Yavari, Z. Chen, A. V. Thomas, W. Ren, H.-M. Cheng and N. Koratkar, *Sci. Rep.*, 2011, **1**, 1-5.
57. S.-E. Cheon, K.-S. Ko, J.-H. Cho, S.-W. Kim, E.-Y. Chin and H.-T. Kim, *J. Electrochem. Soc.*, 2003, **150**, A796-A799.